Journal of Flow Chemistry (2021) 11:303–319
https://doi.org/10.1007/s41981-020-00138-x

FULL PAPER

Nucleation in continuous flow cooling sonocrystallization for coiled capillary crystallizers

Mira Schmalenberg[1] · Lena K. Weick[1] · Norbert Kockmann[1]

Received: 27 November 2020 / Revised: 21 December 2020 / Accepted: 22 December 2020 / Published online: 24 March 2021

Abstract

Nucleation in continuously operated capillary coiled cooling crystallizers is experimentally investigated under the influence of ultrasound. It was found that there is no sharp boundary but rather a transition zone for nucleation under sonication. For this purpose, a tube with an inner diameter of 1.6 mm and a length of 6 m was winded in a coiled flow inverter (CFI) design and immersed into a cooled ultrasonic bath (37 kHz). The CFI design was chosen for improved radial mixing and narrow residence time distribution, which is also investigated. Amino acid L-alanine dissolved in deionized water is employed in a supersaturation range of 1.10 to 1.46 under quiet and sonicated conditions. Nucleation is non-invasive detected using a flow cell equipped with a microscope and camera.

Keywords Coiled flow inverter · Continuous nucleation · Cooling crystallization · Minichannel · Capillary flow · Non-invasive nucleation detection · Sonocrystallization

Introduction

The continuous operation of small-scale equipment is of utmost importance for accelerated process development [1–4]. It is not necessary to switch the operation mode from small scale batch to the continuous production of bigger quantities, smallest quantities can already be continuously produced, and similar equipment concepts can be transferred more easily to larger scales [5]. Furthermore, the continuous mode has advantages, such as smaller hold-ups, higher product reproducibility, and space-time-yield [1, 2, 5, 6].

Highlights
- Sonicated continuous flow for nucleation in coiled flow inverter.
- Nuclei detection non-invasive in continuous flow.
- Determination of two primary nucleation thresholds under sonication, one at the lower limit (transition region starts) and one where nucleation occurs in every experiment under given conditions.

Mira Schmalenberg and Lena K. Weick contributed equally to this work.

✉ Mira Schmalenberg
mira.schmalenberg@tu-dortmund.de

✉ Norbert Kockmann
norbert.kockmann@tu-dortmund.de

[1] BCI Equipment Design, TU Dortmund University, Emil-Figge-Straße 68, 44227 Dortmund, Germany

For continuous operation in crystallization, many aspects have to be considered. Clogging should be avoided, while a narrow crystal size distribution (CSD) is targeted to simplify and minimize post-crystallization operations [7, 8]. In addition, high yield, high purity, and specific particle morphology are often required for sufficient product quality. To avoid the preparation of seed crystals some concepts have already been developed to integrate the nucleation into the crystallization process [9–14].

The concept of continuous nucleation by sonication at continuous flow with good mixing caused by the coiled flow inverter (CFI) design is evaluated in more detail in this contribution. The main goal here is to design an apparatus concept that allows for the non-invasive observation of nucleation due to sonication. In the long term, this forms a database which will enable a suitable operation for the production of continuous seed crystals.

Mechanisms of sonocrystallization in solution

The application of ultrasound for process intensification is a frequently used and increasingly popular tool [15, 16]. Ultrasound is defined as sound waves in a frequency range of 16 kHz to 500 MHz [17]. For the transmission of these waves a medium, for example water, is always required [18]. It is assumed that two phenomena occur simultaneously

but can vary strongly depending on the conditions. On the one hand, ultrasound can cause increased molecular movement in the fluid, which can lead to an increase in the mass transfer as well as increased mixing [19]. On the other hand, acoustic cavitation bubbles are generated by the impact of ultrasound [20]. A detailed description of cavitation bubble formation is given in [21–23]. These cavitation bubbles collapse almost immediately after they are formed [16, 23], which leads to local maxima in temperature, while pressure hotspots occur during this process [21]. Several theories describe the mechanism of nucleation by cavitation, but "there is still no consensus on the fundamental mechanism of ultrasound action on the crystallization process" [16]. The possible processes that are probably influenced by ultrasound during the crystallization process are briefly described here and more detail on the processes can be found in [16].

Concerning the primary homogeneous nucleation, it is difficult to observe it because there can always be the smallest impurities in the system, which would mean heterogonous nucleation was detected. A presumed mechanism for homogenous nucleation is the "segregation theory", where it is assumed that crystal clusters are formed under the effect of an acoustic pressure gradient until they result in a larger crystal [16, 24–26]. Other studies show that the acoustic irradiation leads to overcoming of the critical growth energy [16, 27–29]. Most authors postulate that heterogeneous primary nucleation by sonication is present instead of homogeneous primary nucleation. It is assumed that the reactor surface and smallest impurities can reduce the surface energy barrier [16, 30]. Additionally, dissolved gases in the liquid could act as cavitation nuclei [19]. Therefore, degassing of the solution or filtering can reduce cavitation bubble formation [16, 31]. Inversely, investigations on gassing crystallization have shown that active gassing of a solution can lead to results similar to those of sonocrystallization [32, 33].

The investigations on cavitation bubble formation using sonochemiluminescence by Sarac et al. [34] showed bubble formation solely using free interfaces generated by slug-flow. A coiled perfluoroalkoxy alkane (PFA) tube with an inner diameter of 0.8 mm was placed in an ultrasonic bath (27.2 kHz) [34]. No cavitation bubble formation was observed without the introduction of a gaseous phase [34].

Regarding secondary nucleation, it is assumed that ultrasound increases erosion, fracture, and abrasion, resulting in the formation of new nucleation clusters [16, 35]. This increase is due to better mixing by ultrasound, which inter alia increases the possibility of crystal collision. However, the same mixing effects produced with ultrasound may not produce the same results as mechanical mixing [16, 30, 36, 37]. During crystal growth and agglomeration or fracture, the mechanisms "sonofragmentation, sono-deagglomeration and sonoagglomeration" can be observed, a more detailed description can be found in Nalesso et al. [16]. Different types of fragmentations occur for transient and stable cavitation [38]. With the distinction between transient and stable cavitation, the transient cavitation was observed at 30 kHz and from 41 kHz to 1.14 MHz there is a rather stable cavitation [16]. The collapse intensity of cavitation as well as the active bubble size and its distribution depend on the ultrasound frequency, the energy, and the solution itself [16]. Additionally, it has already been found as rule-of-thumb 35 $W \cdot L^{-1}$ (for most solvents operating at room temperature) [15] must be present for cavitation bubbles to form [17, 19].

Influence parameters of sonocrystallization

Parameters that can be varied and adjusted from the external environment are the ultrasonic hardware, the frequency, the ultrasound exposure, the energy input, and the supersaturation. Depending on these parameters the induction time, the meta stable zone width (MZW), the nucleation rate, the polymorphism, the yield, the crystal size, and its distribution can be influenced. The different ultrasonic system types are ultrasonic baths, which were originally manufactured for equipment cleaning, probe (horn) systems, and planar transducers [17, 21]. The most important advantage of the ultrasonic horn and plate is that the ultrasound can be induced more effectively and with a better focus [12, 39]. The main advantage of the ultrasonic bath is that it is standard laboratory equipment, which is often already available and has not to be purchased separately.

The frequency is an important setting for sonocrystallization because it can affect the bubble dynamics [21, 40], which can affect the crystallization, too. The MZW could be reduced in comparison to silent conditions for different frequencies (range of 41–1140 kHz) with constant calorimetric power [41]. The higher the used frequency, the less the MZW could be reduced [41]. If the applied frequency is decreased the formed crystals become smaller [42]. Nevertheless, Kim and Suslick point out that "the number of cavitating bubbles is not controllable, and so it is exceedingly difficult to compare different frequencies due to changes in the number of cavitating bubbles, which are highly dependent on the specific apparatus used" [21]. Besides the frequency, the intensity is an often-used setting for sonocrystallization investigations. In general, it was determined that crystals become smaller with increasing US intensity [21].

Since in this work an ultrasonic bath was used that has frequency and intensity pre-set, the settings which are more independently adjustable will be discussed. This includes for example the acoustic irradiation time. It was found that with increasing sonication time the crystal sizes decrease and become more uniform [21, 43, 44].

The energy input is another important setting that should always be taken into account when considering sonocrystallization [17]. In most cases, this parameter results from the design of equipment and the hardware used including ultrasound intensity and frequency. However, it can also be set

constant to explicitly exclude this influence [41]. Miyasaka et al. and Kurotani et al. explicitly investigated the influence of the input calorimetric energy in connection with primary nucleation [27, 29]. The calorimetric energy P_{cal} is determined according to Eq. (1) by recording the temperature T change in the medium as a function of time t and by multiplying the heat capacity c_p of the fluid and the heated mass m.

$$P_{cal} = \frac{dT}{dt} c_p m \tag{1}$$

For two amino acids, for example, it was found that there is a local maximum for induction time depending on the ultrasound energy, which in turn is dependent on the degree of supersaturation and the model system used [27]. The supersaturation itself is also an externally adjustable influencing setting. Jordens et al. showed that the greater the supersaturation, the smaller the crystals become, whereby an asymptote was detected from supersaturation of 1.56 [42]. Target parameters that are influenced by ultrasound are induction time, the MZW, the nucleation rate, the polymorphism, yield, particle size, and its distribution along with other interactions generated by ultrasonic irradiation [16].

Ultrasonic irradiation affects the induction time not only for anti-solvent crystallization [44, 45] but also for cooling crystallization [27, 46] and usually shortens the induction time probably due to the better micro-scale mixing and the turbulent flow generated by the acoustic cavitation [21].

The MZW also decreases under the influence of ultrasound [41, 46, 47]. It was found that higher reduction of MZW was achieved at low frequencies (41 kHz) [38]. The nucleation rate is presumably increased because the critical excess free energy is reduced, as the molecule is only surrounded by solution on one side and is in contact with the cavitation bubble on the other [21]. Secondary nucleation is also increased because mixing is improved and the number of collisions is raised [21].

So far unknown is the effect on polymorphic forms by sonication, it is just determined that ultrasound can affect the polymorphic form [46, 48–50]. A further product-determining factor is the yield, which can be higher with acoustic irradiation because ultrasound reduces induction time so nucleation begins earlier [51, 52]. The particle size and its distribution is a very important quantity, also for further processing, so this is a widely studied parameter [27, 40, 42, 43, 51, 53]. Besides, other interactions can be influenced by ultrasound for example interparticle collision, direct interaction between particles, and shockwaves [21, 37].

Continuous sonocrystallization in capillaries

Since there are already some studies on nucleation by the influence of ultrasound irradiation, the most important ones, considering the setup featured in this work, are presented here. Already in 2010, an Ultrasonic Oscillatory Baffled Reactor was patented, which is equipped with an ultrasonic transducer and designed with a continuous flow, mainly used for nucleation [54].

Narducci et al. were among the first to design a continuously (10–30 mL min^{-1}) operated and with 20 kHz ultrasonic processor sonicated stirred vessel (300 mL). In this study, the influence of the duration of exposure, the achievement of the steady-state, the crystal habitus, and the particle size distribution were already examined. They found out, that the particle size under sonication resulted in smaller crystals [43].

Kudo and Takiyama [55] investigated the generation of crystal nuclei for anti-solvent crystallization in segmented flow in a metallic and a flexible tube (last one for connection), each with an inner diameter of 2.4 mm. The metallic tube (L = 0.5 m) was coiled into a 42 kHz ultrasonic bath [55]. The main results were that monodispersed crystal size distribution (CSD) was created [55]. Further investigations on ultrasonic anti-solvent crystallization in milli structured equipment can be found in [56, 57] from the van Gerven group.

At about the same time the research group of Gruber-Woelfler worked on continuous cooling crystallization of acetylsalicylic acid in ethanol using slug-flow and sonication with a flow rate of 6 mL min^{-1}. The coiled polysiloxane tube with an inner diameter of 2 mm and with 1.5 m length was inserted into a 35 kHz ultrasonic bath. One point of investigation was the nearly constant CSD over the required time (25 min). The segmented flow was implemented after the nucleation section and it followed a coiled tubular crystallizer at four different temperature stages. For the whole crystallization process, different seed loadings were investigated with their influence of a fine dissolution after the ultrasonic bath. Furthermore, they analyzed the effect of different ratios of seed-mass and the effect of ultrasound on the product crystals itself. The authors could show that it is possible to design a continuously seeded flow-through crystallizer with in-situ seed generation from ultrasound resulting in a constant seed quantity and quality [11].

A subsequent study, also by Khinast's research group, investigated the controllability of crystal size in the continuous tubular crystallizer. They used the same tubes (d_i = 2 mm, polysiloxane) for the coiled crystallizer and the same cooling crystallization model system (acetylsalicylic acid, ethanol). However, the seed generation via ultrasound was done in a round-bottom flask in 500 mL, which was embedded into the ultrasonic bath (35 kHz). Here the supersaturation $\overline{u}$ was given and the ultrasonic irradiation duration was 60–70 s. The feed solution flow rate was 22 mL min^{-1} and the seed suspension flow rate was 6 mL min^{-1}, these both flows were mixed before entering the crystallization section (three thermostat baths each with 5 m coiled tube). At the outlet, the CSD was evaluated and the crystal size could be controlled by varying the volume flow rate of the seeds. To

avoid clogging, the crystallizer was rinsed with solvent approximately every 10 minutes [13].

Nucleation experiments for different supersaturations in a range from 1.12 to 1.81 were carried out in another milliscale apparatus, a glass flow cell connected to a PFA tube (d_i = 5 mm), and a stirred vessel, here for the model system paracetamol in water. The ultrasonic source was an ultrasound transducer (20 kHz), which was mounted on the glass flow cell or on the stirring tank. The flow rate was selected to be 100 mL min^{-1}. With ultrasound, nuclei could be generated already from supersaturation of 1.32, and under silent condition a supersaturation of 1.87 was necessary [42].

Rossi et al. [58] investigated non-invasive with a high-speed microscope cooling sonocrystallization of adipic acid in water in diverse supersaturations with a sonoprobe (20 kHz). They used a straight process tube made of PFA with an inner diameter of 1 mm and investigated liquid-liquid slug-flow with n-hexane as an inert carrier fluid with a flow rate of 0.3925 mL min^{-1} [58].

Another research group has recently released a patent, it comprises the inlet of a substance to be crystallized into a tubular crystallizer which is sonicated (20 to 40 kHz) by an ultrasonic source and includes a temperature control structure for cooling the process fluid [59]. Studies on this patent were made by Han et al. and Ezeanowi et al. [52, 60].

Han et al. use three ultrasonic baths (35 kHz) connected in series and equipped with thermostats. In each ultrasonic bath, a 12 m or 18 m coiled stainless-steel tube with an inner diameter of 4 mm was inserted. Three different substance systems namely potassium sulfate, copper sulfate, and phthalic acid dissolved in water were examined for cooling crystallization. The mass flow rate was 75 mL min^{-1}. The residence time dependence, the cooling strategy, the influence of supersaturation (1.2, 1.36, 1.54, 1.71, 1.77, and 1.9), and the acoustic irradiation itself were investigated. No usable crystals could be produced without sonication. Additionally, no nuclei were formed at a supersaturation of 1.2, and the system was blocked at a supersaturation of 1.9 [52].

Ezanowi et al. investigated a bigger version of the setup in pilot scale with an inner diameter twice as large and approximately equal length. They found out that with increasing residence time the CSD decreased and that ultrasound prevented pipe clogging [60].

In most of the studies, few information was provided on how exactly the tube was coiled. In addition, the analysis was usually carried out offline, for example by collecting the product solution in a filter or by using a temperature-controlled collecting-vessel, which both does not display the in-situ moment. In all the studies described, the analyses have been carried out for selected supersaturations, but it has not been investigated whether there is a transition or a precise boundary from which nuclei are generated by ultrasound. To fill the gaps addressed here, this work was performed. Under exact choice and description of the winding type, which will be described in more detail below, this and the associated flow conditions are simply repeatable. The non-invasive and in-situ analysis of the crystals by image analysis ensures that really only crystals are produced in the apparatus and not in the periphery. The investigations also close the gap that, until now, crystallization investigations have only been studied for selected supersaturations and not for a merging range. This shows that due to the stochastic process of nucleation, there is no clearly defined boundary between no crystal formation and crystal formation. The choice for the continuous mode of the experiments is not only the basis to construct a seed crystal unit, but also takes advantage of the fact that many individual batch experiments can be replaced by less continuous runs.

Fluid dynamics in a coiled flow inverter

Many of the discussed research projects used a coiled pipe or tube for the process flow. It is space-saving and the flow itself exhibits good radial mixing. In capillaries, the velocities are usually low with laminar flow, hence, in the macroscopic view, there is low radial mixing in the flow of straight capillaries [61].

To create a macroscopic exchange in the flow, coiled tubes are used, especially coiled flow inverters (CFI). They are constructed of helical segments with a minimum of three turns and the segments are linked by 90° bends. The coiled structure itself generates a centrifugal force on the flow, which causes radial mixing, the so-called Dean vortices. Due to the 90° bends the direction of the Dean vortices is changing so the radial mixing is improved [62].

Many investigations about coiled tubes and CFIs have been made, especially in characterizing the improved mixing and the residence time, which could be narrowed by using a CFI instead of a straight tube [62–67]. Some studies have used the CFI design for precipitation [68, 69] or crystallization [70–72].

The main key numbers used to describe a CFI are briefly presented here. The Dean number Dn describes the intensity of the Dean vortices formation (Eq. (2)). It is defined as Reynolds number Re multiplied with the square root of the ratio of the inner diameter d_i to the coil diameter d_c.

$$\mathrm{Dn} = \mathrm{Re} \cdot \sqrt{\frac{d_i}{d_c}} \tag{2}$$

The Reynolds number is known as the ratio of inertia force to frictional force (Eq. (3)) and described as mean velocity $\overline{u}$ multiplied with liquid density ρ_l and characteristic length, here the inner diameter, divided by the dynamic viscosity of the liquid η_l [61].

$$\mathrm{Re} = \frac{\overline{u}\rho_l d_i}{\eta_l} \tag{3}$$

To ensure a narrow residence time distribution in a CFI, various requirements must be fulfilled. The Dean number has to be equal to or higher than three [73], the number of turns has to be equal to or more than five [73], and the number of bends has to be equal to or more than three [62]. Additionally, the modified torsion number T^*, see Eq. 4, has to be equal or higher than 1000, where $\overline{t}$ is the helix pitch [63, 68].

$$T^* = \mathrm{Re} \cdot \frac{\pi \mathrm{d_c}}{\mathrm{p_h}} \tag{4}$$

If solids are present in the flow, it is important to avoid clogging, a homogeneous suspension flow must be ensured, and no particles should sediment. With an empirical correlation based on the tube inner diameter, the mean particle size, the particle mass fraction, the suspension flow rate, and the pulsation characteristics (using a peristaltic pump), a homogeneous suspension flow could be proclaimed. To ensure homogeneous suspension flow, the critical Froude number $\mathrm{Fr_{d,crit}}$, which was developed as an empirical correlation, can be determined to find out, which maximum mean particle size can be transported homogeneously in the tube with a given solid mass fraction. In Eq. (5), the empirical correlation for the critical Froude number is given with model parameters for the switch from moving sediment flow to homogeneous suspension flow [74].

$$\mathrm{Fr_{d,crit}} = 0.252 \cdot \mathrm{Re}^{0.717} \cdot (1 - w_s)^{-4.564} \tag{5}$$

With the usual definition of the densimetric Froude number (Eq. (6)), the maximum mean particle size x_{50} can be determined by converting Eq. (6). The necessary variables are the Reynolds number, the used solid weight fraction w_s, the mean velocity of the process flow, the liquid density, the density difference between the solid and the liquid phase $\Delta\rho_{sl}$ and the acceleration of gravity g [74].

$$\mathrm{Fr_d} = \frac{\overline{u}^2}{x_{50,3} g} \cdot \frac{\rho_l}{\Delta\rho_{sl}} \tag{6}$$

Experimental section and methods

This contribution presents an experimental setup of a coiled tube within an ultrasound bath with an adjacent measuring cell below a microscope, which allows in-situ and non-invasive observation of the nucleation. To evaluate the flow conditions in the coiled tube, the residence time behavior is analyzed. Nucleation experiments depending on supersaturation investigated whether there is a nucleation threshold or a transition region. Also, particle size distribution, pressure loss, and the time till clogging appears are examined and evaluated.

The CFI Design was chosen for its good mixing properties and the low space consumption caused by the coiled tube. The experimental design is described below. The small inner diameter (d_i = 1.6 mm) for the process tube was selected due to the need for a sufficiently high flow rate (around 16 g min^{-1}) to guarantee a homogeneous suspension flow (for the chosen model system and 1 w.% solid). Besides, preliminary tests for this combination have already been carried out on a cooling crystallizer [72], which in the future will also be connected to the plant presented here.

After the description of the experimental setup, the analytical methods used are presented and the performance regarding residence time measurements, nucleation experiments, and calorimetric power is described. In this article, water always means deionized water.

Experimental set-up

The structure of the plant is divided into three units (Fig. 1). The first unit consists of the feed and pump unit (FPU), the second is the ultrasonic unit (USU) and the third unit is the product analysis unit (PAU). In keeping with the modular concept, this structure would consist of three Process Equipment Assemblies (PEAs), which could be used as a single module [75].

The FPU consists of two double-jacketed glass storage tanks with a filling volume of either 1 or 3.5 L. Here, the feed solution and the solvent are prepared, for which they are placed on magnetic stirring plates (MR 3001, Heidolph Instruments GmbH und Co. KG, Germany). The storage tanks each contain a triangular magnetic stirring rod (PTFE, 50 mm, Bohlender GmbH, Germany). The tanks are temperature controlled with a thermostat (CC304, Huber Kältemaschinenbau AG, Germany) and they are connected in series (first the feed storage, second the solution storage). The feed tank contains the undersaturated L-alanine water solution, while the solution tank is filled with water for temperature equilibration and cleaning. The solution is pumped via a peristaltic pump (LabDos Easy-Load, HiTec Zang GmbH, Germany), using a Tygon® tube (inner diameter d_i 1.6 mm). To ensure that the solution does not contain particles when it enters the process tube, it is preceded by a filter frit (pore size III, ROBU Glasfilter Geräte GmbH, Germany). The process tube is made of fluorinated ethylene propylene (FEP) (Bohlender GmbH, Germany) and has an inner diameter d_i of 1.6 mm. The FPU is connected with a three-way connector for a pressure sensor integrated to the third link (A-10, WIKA, Germany) to record the pressure loss. The tube from the feed storage to the three-way connector has a length of 1.6 m.

The process tube is coiled in CFI design on a grid basket, which is available for the used ultrasonic bath. This can be seen in Fig. 2 in the upper picture. The total length of the tube is 6.01 m, including 0.19 m for the inlet and 0.22 m for the

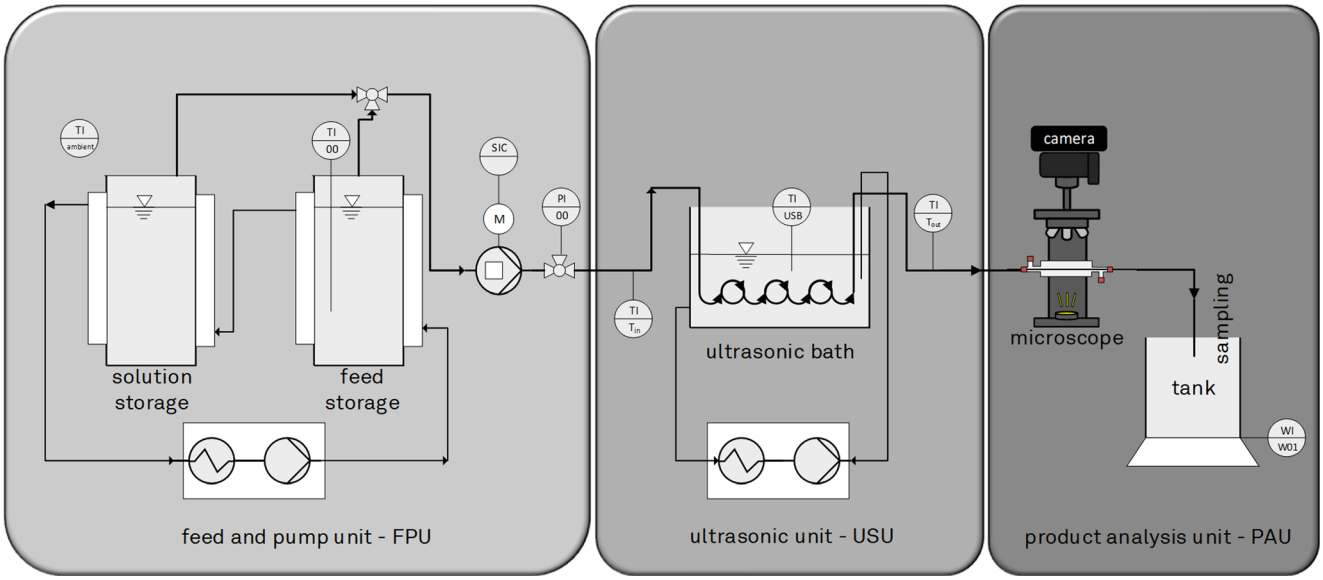

Fig. 1 Experimental Set-Up with three units, feed and pump unit (FPU), ultrasonic unit (USU) and product analysis unit (PAU), process flow from left to right

outlet. The inlet and outlet of the process tube are insulated with polyethylene foam. The CFI winding on the grid is divided into six segments with five turns each. The coil diameter d_c is 52 mm and the distance between the coils, the pitch, is about 3.6 mm. The coiled tube on the grid basket is embedded in the ultrasonic bath (Elmasonic S30H, Elma Schmidbauer GmbH, Germany) filled with deionized water. The bath has a filling volume of 2.75 L [76], whereas it is only filled with 2.19 L so that the coiled tube is always fully covered with water. Moreover, the tube does not touch the ground or walls of the ultrasonic bath. According to the manufacturer, the ultrasonic bath has a frequency of 37 kHz, the total power consumption is 280 W, while 80 W being the effective ultrasonic power [76]. To ensure a constant temperature in the ultrasonic bath for the nucleation experiments, it is connected to a cryostat (Pilot ONE ministat 125, Huber Kältemaschinenbau AG, Germany). The internal pump rate is set to 3000 rpm.

The process tube, which comes out of the USU, is connected to a FEP tube (same inner diameter) of 0.76 m length and leads to the PAU. The next part of the tube (1.2 m) leads from the measuring cell (Fig. 2 bottom) into the sampling tank. The section of the tubing located inside the measuring flow cell has a length of 325 mm. The measuring flow cell in combination with a microscope (Bresser Science ADL 601P, Bresser GmbH, Germany), a photo camera (Nikon Z6, Nikon GmbH, Japan) and an image evaluation tool [77] based on the algorithms of Borchert and Sundmacher[78] and Huo et al. [79] enables a non-invasive in-line measurement of the crystals produced. For further details refer to [77]. The processed fluid is finally collected in a collecting container. This is located on a scale (Kern 572, KERN & SOHN GmbH, Germany) to determine the process mass flow rate from the mass difference with time.

Three resistance thermometers (Pt-B-100-2. RÖSSEL-Messtechnik GmbH, Germany) are used to monitor the temperature with one in the feed or solution storage, one in the ultrasonic bath, and one in the direct environment. Before the experimental runs, all temperature sensors were calibrated by a two-point calibration procedure with two thermostats. The inlet and outlet temperature of the process medium are recorded via sealed thermocouples (Typ K, 1 mm diameter, OMEGA Engineering, United States). From preliminary tests, the following correction Eq. 7 of the measured temperatures on the tube, and the actual temperature could be determined. This correction is valid in the temperature range 10 °C to 60 °C.

$$T_{\text{fluid}}[°\text{C}] = 1.1774 \cdot T_{\text{surface}}[°\text{C}] - 3.9049 \tag{7}$$

For the process control system, a LabManager® (HiTec Zang GmbH, Germany) is used, data evaluation is enabled in LabVision® (HiTec Zang GmbH, Germany). The data is recorded every second.

Measurements

Pressure loss

In addition to temperature monitoring, the pressure loss Δp for the experiments is measured by the pressure sensor (A-10, WIKA, Germany). The pressure loss can also be correlated to the mean flow velocity u according to Eq. (8), where f is the loss coefficient, ρ the fluid density, and L the length of the tube[61].

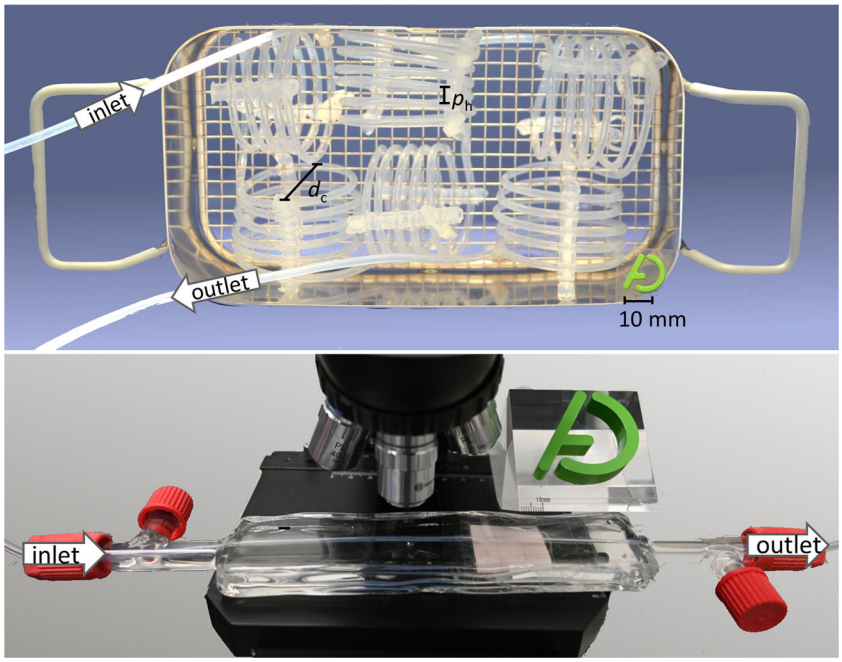

Fig. 2 Process tube coiled on a grid basket in CFI design (upper), measurement cell with process tube under the microscope (bottom)

$$\Delta p = f \frac{\rho L}{2 d_i} \overline{u}^2 \tag{8}$$

A suitable correlation for the friction factor f_a for coiled tubes is Eq. (9) [80] and has already been used successfully in other studies with tubes coiled in CFI design [63, 72]. It is composed of the pipe friction coefficient for straight pipes f_0, with 64/Re for laminar flow, and the Dn number.

$$f_a = f_0 \left(1 + 0.0456 \cdot \mathrm{Dn}^{-0.603}\right) \tag{9}$$

Another correlation for the friction factor f_b for coiled tubes and laminar flow is Eq. (10) [81].

$$f_b = f_0 \left(1 + 0.033 \cdot (\log_{10}(\mathrm{Dn}))^4\right) \tag{10}$$

Both correlations are used and compared with each other in order to enable better predictions to be made for future operations.

Particle measurement via image analysis

To investigate the formed crystals, an image analysis protocol, which was already mentioned in the section above, was used. The special property here is that the crystals can be detected non-invasive without large equipment effort. As a major component, a microscope is equipped with a camera, and a measurement cell is placed below. The process tube is clamped through the measuring cell, which is out of glass and filled with water to observe the crystals distortion-free. Because the system was mostly cooled down to room temperature, no special temperature control of the measurement cell was necessary although this is possible [77].

The photos taken are evaluated using a routine, which is based on the algorithms by [78] and [79]. This semi-automatic image processing routine determines the circular area equivalent diameter, using the projection surface of the crystals [77].

Concentration determination via gravimetric method

A gravimetric method is used to determine and check the dissolved amount of the model substance (L-alanine). Therefore, the quotient of the mass of the target component i and the mass of the solution sol is determined by Eq. (11).

$$w_i = \frac{m_i}{m_{sol}} = \frac{m_{dried} - m_{empty}}{m_{sample} - m_{empty}} \tag{11}$$

An empty (and labeled) 1.5 mL reaction vessel is weighed with a scale (XA 205 Dual Range, Mettler Toldeo, US) to determine m_{empty}. To get m_{sample} a syringe with pre-filter (cellulose acetate membrane, pore size 0.2 µm, VWR International, US) is filled with the solution sample (about 1 mL) and injected into a reaction vessel, and weighed again. After drying the sample in a vacuum drying oven (Memmert VO400, Memmert GmbH + Co. KG, Germany) at 60 °C and with stepwise reduction of the pressure (1 bar, 600 mbar, 300 mbar), it will be weighed again to get m_{dried}. Each sample is dried for a minimum of 14 days and is considered unchanged if the sample does not change for more than 0.001 g, almost the same procedure has already been successfully carried out in [74].

Experimental procedures

First of all, the experimental procedure to determine the residence time of the liquid phase in the USU is described, followed by explaining the performance of nucleation experiments with and without ultrasound. The most important parameters are also defined here. Finally, the procedure is presented for determining the dissipated energy by the ultrasonic bath.

Residence time behavior

To determine the actual liquid residence time t and the distribution sum function $F(t)$, the step-response method was used. For this purpose, deionized water (from solution storage) is first introduced into the entire apparatus (USU). The inlet in the FPU was already filled with tracer solution (from feed storage) up to the second three-way valve (see Fig. 1) in order to measure only the residence time distribution in the USU (pressure sensor was not used here). As a tracer, a thiosulfate solution with a concentration of 0.2–0.4 mg·g^{-1} water (not changing the parameters of water significantly) [73] is used and detected by a UV-Vis detector (Evolution 201, Thermo Fisher Scientific Inc., US). Instead of the microscope in the PAU, the UV-Vis detector with a measuring flow-through cuvette (170700-0.2-40, Hellma Analytics, Germany) is used.

The mass flow rate is set to 16.5 ± 0.8 g min^{-1}. To investigate the influence of the US on the residence time the experiments were done three times without ultrasound and four times with ultrasound. The ultrasonic bath was cooled to room temperature with the connected cryostat.

For calculating the hydrodynamic residence time τ (Eq. (12)), the known geometry of the tube (d_i = 1.6 mm, L = 6 m) for the internal volume V was considered as well as the liquid density ρ_l, which is almost identical to that of water. The values for water are taken from [81].

$$\tau = \frac{V\rho_l}{\dot{m}} \tag{12}$$

The distribution sum curve is defined as Eq. 13, with concentration w at time t in dependence of the tracer concentration w_0.

$$F(t) = \frac{w(t)}{w_0} \tag{13}$$

The actual residence time t (Eq. 14) was determined by integration of the step-response, using the trapezoidal rule. The use of the dimensionless time θ_t (Eq. 15) is used to compare each experiment. With the use of the dispersion model Eq. 16, which allows to consider the axial back mixing, the Bodenstein number Bo was determined by fitting the experimental data using the least square method. This number (Eq. 17) describes the relationship between convective mass transport and axial mixing, which includes the axial dispersion coefficient. It is also used to indicate if axial mixing is negligible compared to convection, i.e. the residence time behavior is comparable with an ideal plug flow (Bo > 100) [74, 82].

$$\bar{t} = \int_{t=0}^{\infty}(1-F(t))dt \tag{14}$$

$$\theta_t = \frac{t}{\bar{t}} \tag{15}$$

$$\mathrm{F}(\theta_t) = \frac{1}{2}\left[1-\mathrm{erf}\left(\frac{\sqrt{\mathrm{Bo}}}{2}\cdot\frac{1-\theta_t}{\sqrt{\theta_t}}\right)\right] \tag{16}$$

$$\mathrm{Bo} = \frac{\bar{u}L}{D_{\mathrm{ax}}} \tag{17}$$

For the description of the residence time distribution in a CFI, it could already be shown that the dispersion model is well suited [72, 74, 83].

Nucleation experiments

An amino acid (L-alanine, purity ≥ 99.6%, Evonik Rexim (Nanning) Pharmaceutical Co., Ltd., China) and water were used for the nucleation experiments with and without ultrasound. Based on the empirically determined solubility curve (Eq. (18)) according to Wohlgemuth et al. [84], the L-alanine/water solution was prepared for the desired saturation temperature T^*.

$$w^*[\mathrm{g}\cdot\mathrm{g_{sol}}] = 0.112381\cdot\mathrm{e}^{\left(9.08492\cdot10^{-3}\cdot T^*[^\circ\mathrm{C}]\right)} \tag{18}$$

The preparation of the solution in the FPU was done one day before the experiments started. Therefore, the feed tank temperature (TI_00) was set to 5 K higher than the chosen saturation temperature (T^* = 50 °C or 60 °C). This ensures that the crystals are all dissolved and that no nuclei were already present in the feed tank. Hence, the solution is not significantly oversaturated before entering the ultrasonic bath. The temperature of the ultrasonic bath was set for each experiment, depending on the target supersaturation, for example to 20 °C (ΔT = 30 K) for a supersaturation of 1.3. To determine the supersaturation from temperature S_T, Eq. (19) was chosen, using the assumption that the activity of the dissolved component behaves ideally [84]. Since this is only a value calculated from the measured temperatures, the gravimetric supersaturation was determined additionally. Therefore, instead of the calculated solved fraction of L-alanine (using Eq. 18), the gravimetrical measured fraction of the feed tank w^* was used. The determined supersaturation is labeled as S_G in the following (Eq. (20)).

$$S_T = \frac{w^*(T^*)}{w(T_{\text{out}})} \tag{19}$$

$$S_G = \frac{w^*}{w(T_{out})} \tag{20}$$

The sonicated and silent nucleation experiments are done in a supersaturation range of 1.10 to 1.36 for a saturation temperature of 50 °C and some extra investigations are made with an inlet saturation temperature of 60 °C for the supersaturation 1.38, 1.42, and 1.46. The supersaturation was adjusted via the end temperature. Before each experiment, the temperature profile runs in with water until it was stationary (for minimum of 20 min) before switching to the undersaturated solution and starting the nucleation experiments, where each experiment is either run till clogging or 20 min if no crystals were visible.

Calorimetric energy input

As already mentioned, Eq. (1) is used to determine the energy input by the ultrasonic bath. This method assumes that the whole power entering the solution is dissipated as heat [42, 85]. Therefore, two setups were used. Case 1 only includes the USU and the 2nd case is the same setup as described in the experimental setup section. In both cases, the ultrasonic bath itself was not temperature controlled via the cryostat.

The environmental temperature, the ultrasonic bath temperature, and in the second case also the in- and outlet temperature of the process flow were measured. In every experiment, the temperature change was recorded in dependency of the time. For every experiment, first, the ultrasonic bath temperature is prepared beneath or at room temperature. Then, the ultrasonic bath was turned on. For the second case, a process flow (water) with room temperature through the CFI tube (16.7 ± 0.1 g min^{-1}) is turned on. Each of these cases were measured four times and for a minimum time of 20 minutes.

The performance of the ultrasonic bath was recorded for comparability with other studies. The measurements showed a temperature change of 0.007 $\text{K}\cdot\text{s}^{-1}$. According to Eq. 1, this results in an energy of 0.35 W applied to the volume of the tube in the ultrasonic bath using the heat capacity of water [81].

Results and discussion

To verify a narrow residence time distribution in the CFI the residence time behavior was investigated. Furthermore, it was evaluated whether it is possible to investigate nucleation in the described setup with and without sonication so that the MZW of primary nucleation can also be determined for continuously operated crystallizers. By non-invasive particle observation, it could be easily detected whether nucleation has occurred in the case of different supersaturations.

Residence time behavior

The residence time distribution of the CFI in the USU is investigated for two reasons. On the one hand, the apparatus is to be characterized entirely and the hypothesis of a narrow residence time will be confirmed by the CFI design. On the other hand, the observations regarding acoustic streaming, mentioned below, made by Valitov et al. [86] will be verified.

The residence time behavior of the tube in CFI design is shown in Fig. 3. Here the residence time sum curve under quiet and sonicated conditions is plotted as a function of dimensionless time, each with the experimental data (symbols) and fitted to the dispersion model (green line). It can be seen that the residence time distribution curve is very narrow and similar to an ideal tube. No optical differences between the silent and sonicated curve can be seen. The most important parameters are listed in Table 1.

The mass flow rate of 16.5 ± 0.8 g min^{-1} could be kept almost constant during the different tests. This allows a good comparison between the silent and sonicated tests. Using the mass flow rate, the Reynolds number, Dean number, and modified torsion number can be determined to 238, 42, and 10,785 respectively. These values show that the flow is in the laminar range and the CFI design fulfills the requirements for a narrow residence time distribution.

The hydrodynamic residence time is slightly shorter than the real evaluated residence times. This could indicate that there might be a small death zone; probably it is the flow-through cuvette in the UV-Vis detector itself. The actual residence times for silent and sonicated conditions are also very similar, both within the error tolerance, but the sonicated one is slightly smaller. The calculated Bodenstein numbers are higher than 100 for both cases, hence, the residence time behavior is similar to an ideal plug flow. Additionally, the one for the sonicated conditions is a bit higher than for the silent, but in the range of the standard deviation, too. Therefore, it can be concluded, that the sonication has no significant effect on the residence time distribution if the CFI design is chosen.

Valitov et al. [86] investigated and evaluated the influence of the ultrasound (horn, 20 kHz) on the flow of a straight FEP tubing with inner diameters of 1.55 mm and 3.2 mm for a sonication time of 0.3, 1.0, and 3.0 s. They assumed that boundary layer streaming could be neglected because FEP as a material is acoustically transparent and boundary layer streaming in millifluidic devices tends to be visible only at higher frequencies (> 1 MHz). Furthermore, they considered and evaluated the Eckart streaming and microjetting, but for the small capillary (1.55 mm), which was also used in this research, the influence of these two flow phenomena, consequently acoustic flow, on the residence time behavior could be

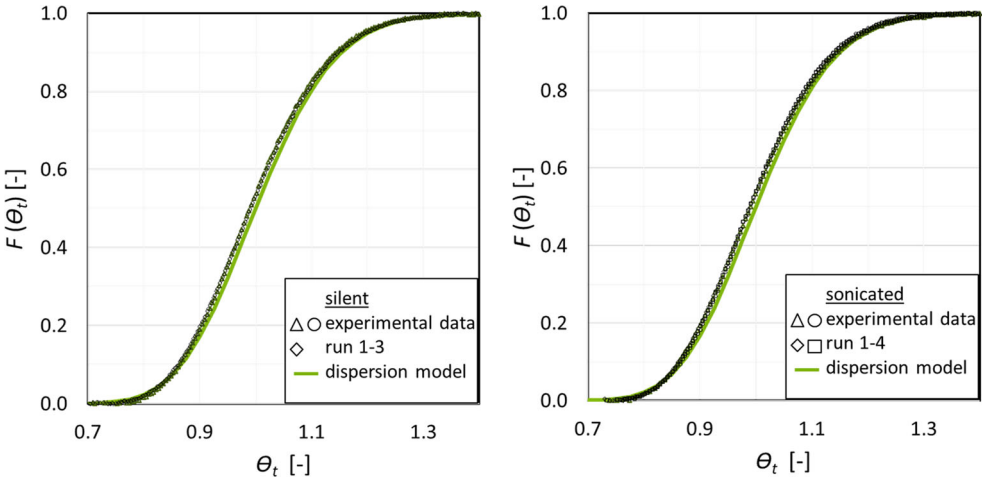

Fig. 3 Residence time sum curve, in dependency of the dimensionless residence time, without periphery for the CFI in the USU for silent (left) and sonicated (right) conditions

neglected. This means that the pure convection model can be applied in the work of Valitov et al. to describe the residence time behavior of the sonicated straight tube of 1.55 mm inner diameter. For the bigger capillary and longer sonication time (3.0 s) the influence of the acoustic streaming could be shown, so the dispersion flow model fitted better than the pure convection model and indicated the presence of axial back mixing due to the sonication, so the residence time behavior was influenced in this case [86].

The results of residence time behavior in the CFI confirms the investigations of Valito et al. [86] and would suggest that the acoustic flow in these capillaries (d_i 1.6 mm) can be neglected. Nevertheless, the small deviations of the actual residence time and the Bodenstein number between the silent and sonicated conditions could be a hint that for small capillaries and longer sonication times a small effect of the acoustic streaming is present.

Nucleation experiments

The nucleation experiments were done under silent and sonicated conditions. To examine whether the nucleation in CFI under ultrasound exposure has a sharp limit or rather a transition area, most of the supersaturations were in the area of 1.10 to 1.46. The supersaturation could not be completely reduced in any of the tests. Accordingly, the indicated supersaturation here always indicated the calculated supersaturation, which is determined from the difference of the saturation and outlet temperature (ΔT) or from the inlet concentration and the outlet temperature. The mass flow rate was set to 17 g min^{-1}.

Figure 4 shows the individually obtained supersaturations. A distinction is made between the sonicated and silent conditions, and some of the individual experiments could be averaged into one sample because of their similarity. The results are divided into three categories. Either no crystals were visible the whole time, crystals were occasionally detected in the transition range, or nucleation crystals were continuously visible. Accordingly, crystal nuclei were repeatedly seen in the transition area during the test, but there were also longer periods (minutes) in which not a single crystal was seen under the microscope. If none of the trials would be assigned to the transition range, there would be a supersaturation threshold above which crystals could always be generated. If there is a transition range, then there are two boundaries: the first between where no crystals are formed and stochastically crystals are formed and the second between stochastically crystals are formed and crystals are visible the whole time.

Assuming that the nucleation behavior of a substance system would be the same in a batch apparatus as in a

Table 1 Key figures for the residence time of the CFI

silent				
$\dot{m}$ [g min^{-1}]	T [°C]	$\bar{t}[s]$	[s]	Bo [-]
16.5 ± 0.8	23.3 ± 0.5	43.8	45.3 ± 0.7	161.5 ± 4.8
sonicated				
$\dot{m}$ [g min^{-1}]	T [°C]	$\bar{t}[s]$	[s]	Bo [-]
16.5 ± 0.8	23.3 ± 0.5	43.8	44.8 ± 0.1	167.1 ± 6.9

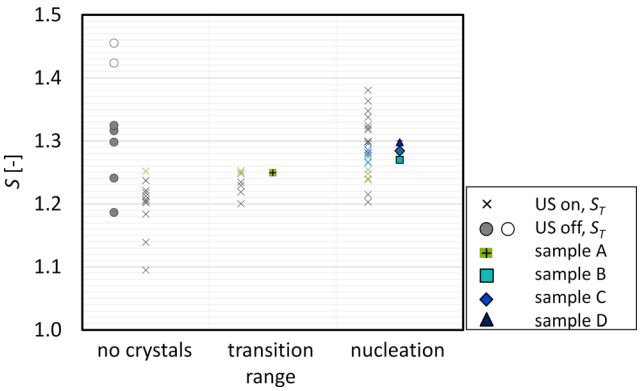

Fig. 4 Nucleation in the USU under sonicated and silent conditions for different supersaturations; samples A – D are averaged values from several experiments at almost the same supersaturation

continuously flowed crystallizer, the following experimental effort between the different modes would result. Each experimental point is run over at least 14 to 20 minutes, with a residence time of 45 s. This results in about 18 to 26 experimental runs. If this were done within a batch experiment, the cooling rates would have to be run in again 18 to 26 times, and after 45 s each time it would have to be determined whether nucleation occurred or not. This shows how much experimental effort can be saved by this newly introduced methodology.

First, for the nucleation experiments without ultrasound, i.e. under quiet conditions, it can be seen that no crystals were visible, neither for the smaller supersaturations in the range of 1.10 to 1.33 ($\Delta T = 10$ K to 34.1 K) and a saturated starting solution at $T^* = 50$ °C (filled grey circles) nor for the higher supersaturations 1.42 and 1.46 ($\Delta T = 34$ K to 41.3 K) with a saturated starting solution at $T^* = 60$ °C (empty circles).

For a continuous stirred tank, which is especially constructed for nucleation of the system used, it is known from the literature [10] that nucleation takes place from subcooling of about 2 K (46 °C to 44 °C, or supersaturation of 1.02) with an induction time of 1.68 min. It should also be considered that for continuously operated crystallizers, not only the MZW can be considered, but also the residence time. Thus, the induction time must be considered and the MZW should therefore be called a primary nucleation threshold (PNT) [10]. Another study investigated the MZW for different saturation and nucleation temperatures for L-alanine/water in a batch stirred vessel [87]. Extrapolation of these data results in a required supersaturation of about 1.4 for an induction time of around 45 s.

The results of the silent nucleation tests suggest that good mixing, produced by the flow in the CFI design, is not sufficient to produce nucleation at lower supersaturations because even at a supersaturation of 1.46 there were no nuclei visible. Presumably, the PNT for silent conditions is even wider. However, this was not considered further, since Eder et al. [11] already found that for the generation of seed crystals in a tube without ultrasound, the system usually clogs.

Every single experiment under sonication is marked as x and sorted into the categories for the different (temperature) supersaturations in Fig. 4. Considering this arrangement, it was found that in a supersaturation range of 1.20–1.25 individual experiments are sorted into all three categories. Accordingly, PNT was significantly reduced by sonication of the tube. No special effect could be determined regarding the experimental days or the ambient temperature. Therefore, the results show that under the selected process conditions of flow rate (17 g min^{-1}) and used experimental setup there is no precisely defined supersaturation threshold above which nucleation is generated by ultrasound, but rather a transition region. This could be because both nucleation and the formation of cavitation bubbles are stochastic processes. It is also known that cavitation bubbles are size distributed, which in turn leads to size distribution of crystal nuclei.

When interpreting the results, it should be considered that the influence of a different residence time and, consequently, a longer possible induction time has not been investigated, because of the given boundary conditions (mass flow rate and manageable coiling length of the tube). If the residence time in the ultrasonic bath could have been extended by a longer tube, Fig. 4 would probably have changed that crystals also have been seen at lower supersaturations or the transition range would have been smaller, since the possible induction time could be longer.

Since eight experiments were performed with approximately the same supersaturation of 1.25, these experiments were combined as sample A, and shown as a cross with a green background (Fig. 4). This means that the S_T and S_G of these tests are averaged as well as their mass flow rate, ambient temperature $T_{ambient,}$ and the determined and calculated pressure loss. These values are listed in Table 2. This averaged sample A consists of one experiment, in which no crystals were visible, three experiments, in which crystals were partially visible, and four experiments with sustained nucleation. This leads to the conclusion that for the selected material system and the apparatus arrangement the transition to a most probable formation of crystal nuclei is present from supersaturation of 1.249 ± 0.005.

For other supersaturations in the nucleation range, experiments could be combined into one to compare these points with each other in a more targeted way. For this purpose, at least three experiments were averaged, which are also listed in Table 2 with their associated process variables. In the diagram, these samples B – D are also shown as blue symbols. In summary, it is shown as described before that lower supersaturations are required for nucleation by sonication than without. Further, it was found that there is a transition area, in which nucleation takes place in the selected apparatus and chosen model system. For the selected conditions it is found that the PNT starts at a supersaturation of 1.2 and above a supersaturation of 1.26 crystallization always occurs.

In comparison to the data from the literature [42, 52, 58], these results could indicate that using lower frequencies in the rage of 20–40 kHz, a critical nucleation threshold in a supersaturation range of 1.25 to 1.3 is present. To verify this statement, more investigations should be carried out with the same equipment and the same energy input for many different substance systems.

The results also confirm the hypothesis that nucleation is caused by the cavitation bubble rather than by the acoustic flow, because the frequency range used is known for pronounced cavitation bubble formation [16]. Additionally, Valitov et al. [86] showed that acoustic flow is rather negligible for this capillary size, and even with an already very well-mixed system, generated by the tube design, the PNT could

Table 2 Averaged nucleation experiments in the USU under sonicated conditions for different supersaturations

	number of experimental runs	S [-]	$\dot{m}$ [g min^{-1}]	$T_{ambient}$ [°C]	*status*	Δp_{exp} [mbar]	Δp_{calc} [mbar] with f_a	Δp_{calc} [mbar] with f_b	$\Delta \overline{p_{calc}}$ [mbar]
A	8	1.249±0.005	17.2±0.3	23.5±1.0	transition range	195.5±6.8	181.1	214.7	197.9
B	3	1.270±0.005	17.3±0.4	23.5±0.3	nucleation	199.5±6.9	184.9	218.8	201.9
C	4	1.284±0.005	17.3±0.3	22.9±0.9	nucleation	206.5±6.6	188.9	222.5	205.7
D	4	1.298±0.003	17.3±0.3	23.2±0.9	nucleation	213.1±8.7	190.6	224.5	207.6

not be reduced. However, no cavitation bubble formation could be observed in a smaller capillary (d_i = 0.8 mm) without air slugs in the investigations of Sarac et al. [34]. In order to ensure that cavitation bubble formation is responsible for nucleation, it should be investigated if cavitation bubbles are formed in the capillary size of 1.6 mm.

Crystal size distribution

To compare the samples A – D, the relating CSD was also investigated. In addition, another single experiment with supersaturation of 1.38 was added for evaluation. Photos were taken at random times during the experiments, at least with a time interval of three seconds to ensure that no crystals are photographed twice. Crystals with a diameter of less than 10 µm were not included in the evaluation, as the image analysis could not determine whether these were actually formed crystal nuclei or only image artifacts. These random photos were evaluated using the image evaluation tool described above [77]. The results are shown in Fig. 5. The determined supersaturation is plotted as dependence of the diameter. This is the circular equivalent diameter. The number of optically evaluated particles is listed above each CSD. The crystal size distributions are drawn in classes (black points, with a class width of 10 µm) and as boxplots.

Based on the CSD results, no clear influence between supersaturation and the influence on crystal size can be identified. For the lower supersaturations (< 1.3) a particularly larger amount of fine grain (< 25 µm) was detected. This can also be seen in the small values for $x_{10,0}$. The mean crystal size is between 24 and 49 µm. At the higher supersaturation single experiment, the particles are bigger and the $x_{50,0}$ is 62 µm. However, since a very different number of crystals were evaluated in each experiment, an interpretation of the dependence between supersaturation and crystal size is not statistically validated. For this reason, the only conclusion to be drawn from these results is that crystals with a size of 10–150 µm were produced, but the majority of them are below 100 µm. Therefore, the created crystals are in the same range of crystal size as they were created by Eder et al. [11] with a different model system, but in most similar conditions.

Pressure drop and clogging

The experimentally determined pressure loss Δp_{exp} is compared to the calculated one. Figure 6 shows the measured pressure loss (filled rhombus), the calculated pressure loss coefficient f_a (squares) and f_b (triangles) and the averaged pressure loss from both (plus sign) over the Reynolds number. It can be seen that the actual pressure loss with loss coefficient f_a calculated is too low and f_b is overestimated. Averaging the two calculated pressure losses gives a better prediction of the pressure loss for the range investigated here. This calculation can help to follow an automated operation by starting a flushing cycle in case of deviating pressure loss.

For most of the nucleation experiments, the time of clogging was also recorded, shown in Fig. 7. The shortest test duration was thus about 14 min and a maximum of 35 min. Dependence of the supersaturation on the clogging time t_{clog} could not be detected, because both extrema could be found at the same supersaturation. The mean time until clogging was 22 min. Although a clogging is usually visible due to the transparent tube, no location could be identified where clogging has repeatedly occurred. Additionally, it was not possible to identify excessive solid loads, which could be the cause of clogging. It is assumed that the small particles (< 90 µm), which tend to agglomerate more frequently [88], have caused the clogging, although the homogeneous flow conditions are fulfilled. Besides, the already formed crystal nuclei can lead to a strengthening of secondary nucleation, because not enough surface for the crystals to grow is available and, instead, secondary nucleation occurs, which leads to clogging due to the relatively high supersaturation.

A similar experimental setup to ours can be found in the work of Furuta et al. [89] with a pH swing crystallization. Here, a coiled tube made of PFA (d_i = 2 mm) and a length of 20–40 m was inserted into a temperature-controlled ultrasonic bath (40 kHz). The flow rate was set to 50 mL min^{-1}. However, the influence of ultrasound on the formation of nuclei was not investigated by the authors. The ultrasonic irradiation was only used to avoid clogging [89].

In other research groups, too, observations have been made on clogging. For example, Eder et al. [11] could not achieve stable seed crystal formation without ultrasound. Likely,

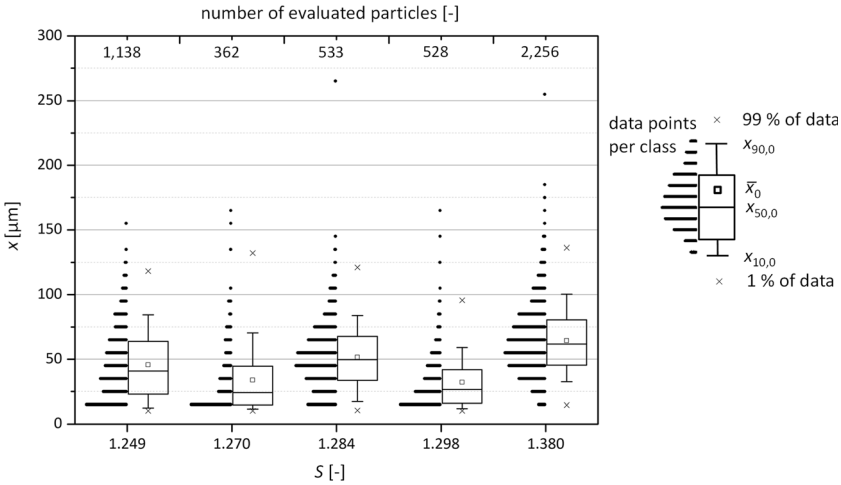

Fig. 5 Crystal size distribution, evaluated with image analysis, in dependence of the supersaturation (for averaged nucleation experiments (A-D) and one additional experiment with higher supersaturation (1.38))

direct clogging would also have occurred in our case if even higher supersaturations had been applied to produce crystals without ultrasound. In the investigations of Han et al. [52] a feasible, stable operation was defined, if 3 to 4 residence times no clogging occurred. According to this definition, all experiments presented here would have run stably. However, this cannot be compared directly because the diameter chosen by Han et al. is 4 mm [52]. But, their average velocity is in a comparable range from 8 to 16 cm s^{-1} [52] to ours of around 13 cm s^{-1}. They also found that supersaturations that are punctual high and not uniformly distributed lead to clogging. In the case of Ezeanowi et al. [60], no clogging was observed at similar average velocities of 5–9 cm s^{-1} and an internal diameter of 250 mm. The observed duration per experiment was also 3–4 residence times [60].

In combination with the results determined here, it can be assumed that clogging can be prevented with even higher suspension flow, despite the previously mentioned process condition of homogeneous suspension. As an alternative to avoid clogging problems, a feed mixture with a solution and seed suspension can be used, or rinse cycles can be implemented as Besenhard et al. [13] did. It is interesting to note here that the rinse cycles were scheduled after 10 min [13], i.e. in a similar time range as our shortest run till clogging was observed. If stable nucleation operation without clogging is guaranteed, the USU presented here can be used as a seed crystal generation unit for continuous crystallization equipment as known from [71, 72, 90–93].

Conclusions

Cooling crystallization was investigated within a capillary coiled flow inverter (CFI) with a tube diameter of 1.6 mm embedded in an ultrasonic bath for nucleation in a continuous flow with different supersaturations. For this purpose, the outlet of the test facility has been equipped with a non-invasive flow cell under a microscope with a conventional photo camera. The CFI design ensures a very narrow residence time behavior of the liquid phase. At a mass flow rate of 16.5 g min^{-1}, a Bodenstein number of approx. 161–167 was obtained with a residence time in the ultrasonic bath of 45 s. Only very slight differences between the residence time under

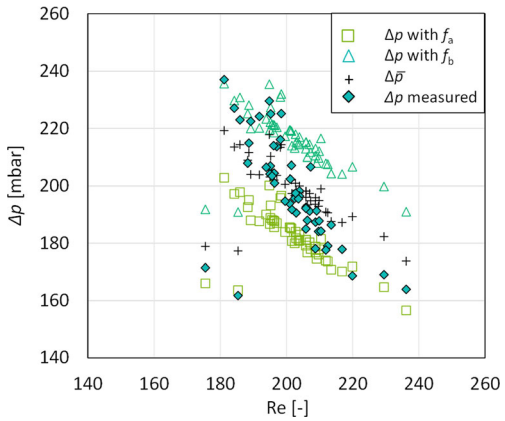

Fig. 6 Measured and calculated pressure loss in dependence of the Reynolds number

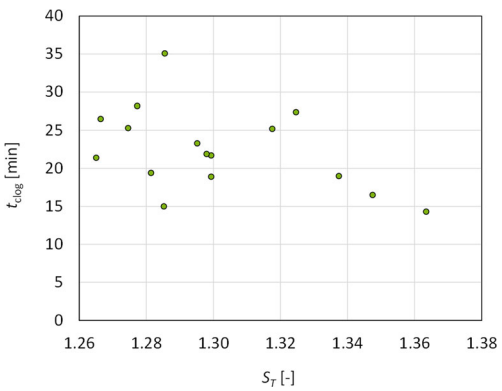

Fig. 7 Time of clogging after starting the process solution for the respective supersaturation

sonication and quiet conditions could be detected which could indicate an influence of the acoustic streaming.

Under silent conditions, no nucleation was observed in the investigated range of supersaturation from 1.10 to 1.46 for the model system L-alanine/water. The first nuclei could be detected under sonication and supersaturation of 1.2. The results of the nucleation experiments show that under the selected conditions (ultrasonic bath, CFI designed tube, L-alanine/water, and residence time 45 s) the primary nucleation threshold (PNT) could be reduced by ultrasound as expected. Additionally, no rigid threshold for nucleation could be found, but a nucleation range was identified in the investigated setup. Nucleation was detected for supersaturations larger than 1.25. The transition range indicates that the two stochastic processes of cavitation bubble formation and nucleation must be sufficiently pronounced to ensure nucleation. No influence of the set supersaturation could be determined on the crystal size distribution or the time until clogging. The minimum time until clogging occurred was 14 minutes. The crystal size is in a range from 10 to 150 µm, where the most are from the size in the range of 24–49 µm after a residence time of 45 s.

Overall, the investigated setup is suitable for the rapid detection of the influence of supersaturation on material systems by sonication. This setup consisting of coiled polymer capillary within an ultrasound bath can easily be set up with existing laboratory equipment. The developed measuring cell from a glass jacket, optical microscope, and digital camera could even enable to identify influences on crystal form quickly and easily by ultrasound. In addition, the ultrasonic unit (USU) can be used as a seed crystal production unit and in combination with rinse protocols for a combination of continuous crystallization for the small-scale with other crystal growth units.

Acknowledgements The authors would like to thank Prof. Dr. Gerhard Schembecker and Dr. Kerstin Wohlgemuth (TU Dortmund University, BCI Laboratory of Plant and Process Design) for their inspiring discussions on the investigations. We would also like to thank the reviewer for the diligent review and helpful comments. Furthermore, we thank our technician Carsten Schrömges for the technical support.

Author contributions The manuscript was written through contributions of all authors. All authors have given approval to the final version of the manuscript.

Funding Open Access funding enabled and organized by Projekt DEAL. This research was funded by the German Federal Ministry of Economic Affairs and Energy (BMWi) and the Project Management Jülich (PtJ) as part of the ENPRO2.0 initiative (Ref. no. 03ET1528A). Additionally, we acknowledge financial support by Deutsche Forschungsgemeinschaft and Technische Universität Dortmund/TU Dortmund University within the funding programme Open Access Publishing.

Compliance with ethical standards

Conflicts of interest/Competing interests No conflict of interest

Competing financial interest The authors declare no competing financial interest.

Abbreviations *CFI,* coiled flow inverter; *CSD,* crystal size distribution; *FPU,* feed and pump unit; *FEP,* fluorinated ethylene propylene; *MZW,* metastable zone width; *PFA,* perfluoroalkoxy alkane; *PNT,* primary nucleation threshold; *PEAs,* Process Equipment Assemblies; *PAU,* product analysis unit; *US,* ultrasound; *USU,* ultrasonic unit

References

1 Ma Y, Wu S, Macaringue EGJ et al (2020) Recent progress in continuous crystallization of pharmaceutical products: precise preparation and control. Org Process Res Dev. https://doi.org/10.1021/acs.oprd.9b00362

2 Yazdanpanah N, Nagy ZK (2020) The Handbook of Continuous Crystallization. Royal Society of Chemistry, Cambridge

3 Melches C, Plate H, Schürhoff J et al (2020) The steps from batchwise to continuous crystallization for a fine chemical: a case study. Crystals 10:542. https://doi.org/10.3390/cryst10060542

4 Zhang D, Xu S, Du S et al (2017) Progress of pharmaceutical continuous crystallization. Engineering 3:354–364. https://doi.org/10.1016/J.ENG.2017.03.023

5 Bieringer T, Buchholz S, Kockmann N (2013) Future production concepts in the chemical industry: modular - small-scale - continuous. Chem Eng Technol 36:900–910. https://doi.org/10.1002/ceat.201200631

6 Schaber SD, Gerogiorgis DI, Ramachandran R et al (2011) Economic analysis of integrated continuous and batch pharmaceutical manufacturing: a case study. Ind Eng Chem Res 50:10083–10092. https://doi.org/10.1021/ie2006752

7 Sun (2010) Particle size specifications for solid oral dosage forms: a regulatory perspective. https://www.americanpharmaceuticalreview.com/Featured-Articles/36779-Particle-Size-Specifications-for-Solid-Oral-Dosage-Forms-A-Regulatory-Perspective/. Accessed 7 Oct 2020

8 Jong EJ de (1982) Entwicklung von Kristallisatoren. Chem Ing Tech 54:193–202. https://doi.org/10.1002/cite.330540303

9 Hohmann L (2019) Process and equipment design for small-scale continuous crystallization, 1. Auflage. Schriftenreihe Apparatedesign, Band 11. Dr. Hut, München

10 Lührmann M-C, Timmermann J, Schembecker G et al (2018) Enhanced product quality control through separation of crystallization phenomena in a four-stage MSMPR cascade. Cryst Growth Des 18:7323–7334. https://doi.org/10.1021/acs.cgd.8b00941

11 Eder RJP, Schrank S, Besenhard MO et al (2012) Continuous Sonocrystallization of Acetylsalicylic Acid (ASA): control of crystal size. Cryst Growth Des 12:4733–4738. https://doi.org/10.1021/cg201567y

12 Jiang M, Papageorgiou CD, Waetzig J et al (2015) Indirect ultrasonication in continuous slug-flow crystallization. Cryst Growth Des 15:2486–2492. https://doi.org/10.1021/acs.cgd.5b00263

13 Besenhard MO, Neugebauer P, Ho C-D et al (2015) Crystal size control in a continuous tubular crystallizer. Cryst Growth Des 15:1683–1691. https://doi.org/10.1021/cg501637m

14 Wong SY, Cui Y, Myerson AS (2013) Contact secondary nucleation as a means of creating seeds for continuous tubular crystallizers. Cryst Growth Des 13:2514–2521. https://doi.org/10.1021/cg4002303

15 Ruecroft G, Hipkiss D, Ly T et al (2005) Sonocrystallization: the use of ultrasound for improved industrial crystallization. Org Process Res Dev 9:923–932. https://doi.org/10.1021/op050109x

16 Nalesso S, Bussemaker MJ, Sear RP et al (2019) A review on possible mechanisms of sonocrystallisation in solution. Ultrason Sonochem 57:125–138. https://doi.org/10.1016/j.ultsonch.2019.04.020

17 Thompson LH, Doraiswamy LK (1999) Sonochemistry: science and engineering. Ind Eng Chem Res 38:1215–1249. https://doi.org/10.1021/ie9804172

18 Edmonds P, Dunn D (1981) Introduction: physical description of ultrasonic fields. In: Edmonds PD (ed) Methods of experimental physics // Ultrasonics. Acad. Press, Academic, New York, pp 1–28

19 Pohl B (2012) Charakterisierung der Mischung und Fällung bei kontinuierlichen sonochemischen Reaktoren unter besonderer Berücksichtigung der Reaktorform. Dissertation, Technische Universität Bergakademie Freiberg

20 Apfel RE. Acoustic cavitation. In Peter D. Edmonds: Methods in experimental physics. Academic Press 19:355–411. https://doi.org/10.1016/S0076-695X(08)60338-5

21 Kim H, Suslick K (2018) The effects of ultrasound on crystals: sonocrystallization and sonofragmentation. Crystals 8:280. https://doi.org/10.3390/cryst8070280

22 Brennen CE (2014) Cavitation and bubble dynamics. Cambridge University Press, Cambridge

23 Leong T, Ashokkumar M, Kentish S (2011) The fundamentals of power ultrasound - a review. Acoust Aust 39:54–63

24 Harzali H, Baillon F, Louisnard O et al (2011) Experimental study of sono-crystallisation of ZnSO4 7H2O, and interpretation by the segregation theory. Ultrason Sonochem 18:1097–1106. https://doi.org/10.1016/j.ultsonch.2011.03.007

25 Dodds J, Espitalier F, Louisnard O et al (2007) The effect of ultrasound on crystallisation-precipitation processes: some examples and a new segregation model. Part Part Syst Charact 24:18–28. https://doi.org/10.1002/ppsc.200601046

26 Grossier R, Louisnard O, Vargas Y (2007) Mixture segregation by an inertial cavitation bubble. Ultrason Sonochem 14:431–437. https://doi.org/10.1016/j.ultsonch.2006.10.010

27 Kurotani M, Miyasaka E, Ebihara S et al (2009) Effect of ultrasonic irradiation on the behavior of primary nucleation of amino acids in supersaturated solutions. J Cryst Growth 311:2714–2721. https://doi.org/10.1016/j.jcrysgro.2009.03.009

28 Miyasaka E, Kato Y, Hagisawa M et al (2006) Effect of ultrasonic irradiation on the number of acetylsalicylic acid crystals produced under the supersaturated condition and the ability of controlling the final crystal size via primary nucleation. J Cryst Growth 289:324–330. https://doi.org/10.1016/j.jcrysgro.2005.11.084

29 Miyasaka E, Ebihara S, Hirasawa I (2006) Investigation of primary nucleation phenomena of acetylsalicylic acid crystals induced by ultrasonic irradiation—ultrasonic energy needed to activate primary nucleation. J Cryst Growth 295:97–101. https://doi.org/10.1016/j.jcrysgro.2006.07.020

30 Hem SL (1967) The effect of ultrasonic vibrations on crystallization processes. Ultrasonics 5:202–207. https://doi.org/10.1016/0041-624X(67)90061-3

31 Lee J (2016) Handbook of ultrasonics and sonochemistry: Importance of Sonication and Solution Conditions on the Acoustic Cavitation Activity. Springer, Singapore

32 Wohlgemuth K, Ruether F, Schembecker G (2010) Sonocrystallization and crystallization with gassing of adipic acid. Chem Eng Sci 65:1016–1027. https://doi.org/10.1016/j.ces.2009.09.055

33 Wohlgemuth K, Kordylla A, Ruether F et al (2009) Experimental study of the effect of bubbles on nucleation during batch cooling crystallization. Chem Eng Sci 64:4155–4163. https://doi.org/10.1016/j.ces.2009.06.041

34 Sarac BE, Stephens DS, Eisener J et al (2020) Cavitation bubble dynamics and sonochemiluminescence activity inside sonicated submerged flow tubes. Chem Eng Process Process Intensif 150:107872. https://doi.org/10.1016/j.cep.2020.107872

35 Hem SL, Skauen DM, Beal HM (1967) Mechanism of crystallization of hydrocortisone by ultrasonic irradiation. J Pharm Sci 56:229–233. https://doi.org/10.1002/jps.2600560216

36 Lee J, Ashokkumar M, Kentish SE (2014) Influence of mixing and ultrasound frequency on antisolvent crystallisation of sodium chloride. Ultrason Sonochem 21:60–68. https://doi.org/10.1016/j.ultsonch.2013.07.005

37 Zeiger BW, Suslick KS (2011) Sonofragmentation of molecular crystals. J Am Chem Soc 133:14530–14533. https://doi.org/10.1021/ja205867f

38 Jordens J, Appermont T, Gielen B et al (2016) Sonofragmentation: effect of ultrasound frequency and power on particle breakage. Cryst Growth Des 16:6167–6177. https://doi.org/10.1021/acs.cgd.6b00088

39 Jiang M, Gu C, Braatz RD (2017) Analysis of focused indirect ultrasound via high-speed spatially localized pressure sensing and its consequences on nucleation. Chem Eng Process Process Intensif 117:186–194. https://doi.org/10.1016/j.cep.2017.04.008

40 Nalajala VS, Moholkar VS (2011) Investigations in the physical mechanism of sonocrystallization. Ultrason Sonochem 18:345–355. https://doi.org/10.1016/j.ultsonch.2010.06.016

41 Jordens J, Gielen B, Braeken L et al (2014) Determination of the effect of the ultrasonic frequency on the cooling crystallization of paracetamol. Chem Eng Process Process Intensif 84:38–44. https://doi.org/10.1016/j.cep.2014.01.006

42 Jordens J, Canini E, Gielen B et al (2017) Ultrasound assisted particle size control by continuous seed generation and batch growth. Crystals 7:195. https://doi.org/10.3390/cryst7070195

43 Narducci O, Jones AG, Kougoulos E (2011) Continuous crystallization of adipic acid with ultrasound. Chem Eng Sci 66:1069–1076. https://doi.org/10.1016/j.ces.2010.12.008

44 Li H, Wang J, Bao Y et al (2003) Rapid sonocrystallization in the salting-out process. J Cryst Growth 247:192–198. https://doi.org/10.1016/S0022-0248(02)01941-3

45 Guo Z, Zhang M, Li H et al (2005) Effect of ultrasound on anti-solvent crystallization process. J Cryst Growth 273:555–563. https://doi.org/10.1016/j.jcrysgro.2004.09.049

46 Gracin S, Uusi-Penttilä M, Rasmuson ÅC (2005) Influence of ultrasound on the nucleation of polymorphs of p -Aminobenzoic Acid. Cryst Growth Des 5:1787–1794. https://doi.org/10.1021/cg050056a

47 Kordylla A, Koch S, Tumakaka F et al (2008) Towards an optimized crystallization with ultrasound: Effect of solvent properties and ultrasonic process parameters. J Cryst Growth 310:4177–4184. https://doi.org/10.1016/j.jcrysgro.2008.06.057

48 Louhi-Kultanen M, Karjalainen M, Rantanen J et al (2006) Crystallization of glycine with ultrasound. Int J Pharm 320:23–29. https://doi.org/10.1016/j.ijpharm.2006.03.054

49 Kurotani M, Hirasawa I (2008) Polymorph control of sulfamerazine by ultrasonic irradiation. J Cryst Growth 310:4576–4580. https://doi.org/10.1016/j.jcrysgro.2008.08.002

50 Hatakka H, Alatalo H, Louhi-Kultanen M et al (2010) Closed-loop control of reactive crystallization PART II: polymorphism control of L-glutamic acid by sonocrystallization and seeding. Chem Eng Technol 33:751–756. https://doi.org/10.1002/ceat.200900577

51 Nguyen T, Khan A, Bruce L et al (2017) The effect of ultrasound on the crystallisation of paracetamol in the presence of structurally similar impurities. Crystals 7:294. https://doi.org/10.3390/cryst7100294

52 Han B, Ezeanowi NC, Koiranen TO et al (2018) Insights into design criteria for a continuous, sonicated modular tubular cooling crystallizer. Cryst Growth Des 18:7286–7295. https://doi.org/10.1021/acs.cgd.8b00700

53 Amara N, Ratsimba B, Wilhelm A-M et al (2001) Crystallization of potash alum: effect of power ultrasound. Ultrason Sonochem 8:265–270. https://doi.org/10.1016/S1350-4177(01)00087-6

54 Ruecroft G, Bruns J (2010) An apparatus and process for producing crystals (WO 2010/079350 A2). Accessed 26 Aug 2020

55 Kudo S, Takiyama H (2012) Production of fine organic crystalline particles by using milli segmented flow crystallizer. J Chem Eng Jpn 45:305–309. https://doi.org/10.1252/jcej.11we168

56 Hussain MN, Jordens J, John JJ et al (2019) Enhancing pharmaceutical crystallization in a flow crystallizer with ultrasound: Anti-solvent crystallization. Ultrason Sonochem 59:104743. https://doi.org/10.1016/j.ultsonch.2019.104743

57 Savvopoulos SV, Hussain MN, Jordens J et al (2019) A mathematical model of the ultrasound-assisted continuous tubular crystallization of aspirin. Cryst Growth Des 19:5111–5122. https://doi.org/10.1021/acs.cgd.9b00466

58 Rossi D, Jamshidi R, Saffari N et al (2015) Continuous-flow sonocrystallization in droplet-based microfluidics. Cryst Growth Des 15:5519–5529. https://doi.org/10.1021/acs.cgd.5b01153

59 Koiranen T, Ekberg B, Häkkinen A et al (2018) An ultrasound crystallization device and an ultrasound crystallization system (WO/2018/096205). Accessed 26 Aug 2020

60 Ezeanowi N, Pajari H, Laitinen A et al (2020) Monitoring the dynamics of a continuous sonicated tubular cooling crystallizer. Cryst Growth Des 20:1458–1466. https://doi.org/10.1021/acs.cgd.9b01103

61 Zierep J, Bühler K (2018) Grundzüge der Strömungslehre: Grundlagen, Statik und Dynamik der Fluide, 11. Aufl. 2018. Springer Fachmedien Wiesbaden; Imprint: Springer Vieweg, Wiesbaden

62 Saxena AK, Nigam KDP (1984) Coiled configuration for flow inversion and its effect on residence time distribution. AIChE J 30:363–368. https://doi.org/10.1002/aic.690300303

63 Klutz S, Kurt SK, Lobedann M et al (2015) Narrow residence time distribution in tubular reactor concept for Reynolds number range of 10–100. Chem Eng Res Des 95:22–33. https://doi.org/10.1016/j.cherd.2015.01.003

64 Mansour M, Liu Z, Janiga G et al (2017) Numerical study of liquid-liquid mixing in helical pipes. Chem Eng Sci 172:250–261. https://doi.org/10.1016/j.ces.2017.06.015

65 Sharma L, Nigam K, Roy S (2017) Single phase mixing in coiled tubes and coiled flow inverters in different flow regimes. Chem Eng Sci 160:227–235. https://doi.org/10.1016/j.ces.2016.11.034

66 Vashisth S, Nigam KDP (2008) Liquid-phase residence time distribution for two-phase flow in coiled flow inverter. Ind Eng Chem Res 47:3630–3638. https://doi.org/10.1021/ie070447h

67 Rossi D, Gargiulo L, Valitov G et al (2017) Experimental characterization of axial dispersion in coiled flow inverters. Chem Eng Res Des 120:159–170. https://doi.org/10.1016/j.cherd.2017.02.011

68 Kurt SK, Akhtar M, Nigam KDP et al (2017) Continuous reactive precipitation in a coiled flow inverter: inert particle tracking, modular design, and production of uniform CaCO 3 particles. Ind Eng Chem Res 56:11320–11335. https://doi.org/10.1021/acs.iecr.7b02240

69 Benitez-Chapa AG, Nigam KDP, Alvarez AJ (2020) Process intensification of continuous antisolvent crystallization using a coiled flow inverter. Ind Eng Chem Res 59:3934–3942. https://doi.org/10.1021/acs.iecr.9b04160

70 Hohmann L, Gorny R, Klaas O et al (2016) Design of a continuous tubular cooling crystallizer for process development on lab-scale. Chem Eng Technol 39:1268–1280. https://doi.org/10.1002/ceat.201600072

71 Hohmann L, Greinert T, Mierka O et al (2018) Analysis of crystal size dispersion effects in a continuous coiled tubular crystallizer: experiments and modeling. Cryst Growth Des 18:1459–1473. https://doi.org/10.1021/acs.cgd.7b01383

72 Schmalenberg M, Hohmann L, Kockmann N (2018) Miniaturized tubular cooling crystallizer with solid-liquid flow for process development. In: Proceedings of the ASME 16th International Conference on Nanochannels, Microchannels, and Minichannels 2018. American Society of Mechanical Engineers Digital Collection; The American Society of Mechanical Engineers, New York. https://doi.org/10.1115/ICNMM2018-7660

73 Kurt SK, Gelhausen MG, Kockmann N (2015) Axial dispersion and heat transfer in a milli/microstructured coiled flow inverter for narrow residence time distribution at laminar flow. Chem Eng Technol 38:1122–1130. https://doi.org/10.1002/ceat.201400515

74 Hohmann L, Schmalenberg M, Prasanna M et al (2019) Suspension flow behavior and particle residence time distribution in helical tube devices. Chem Eng J 360:1371–1389. https://doi.org/10.1016/j.cej.2018.10.166

75 Klose A, Merkelbach S, Menschner A et al (2019) Orchestration requirements for modular process plants in chemical and pharmaceutical industries. Chem Eng Technol 42:2282–2291. https://doi.org/10.1002/ceat.201900298

76 Elma Schmidbauer GmbH (2020) Elmasonic S 30 H: Ultraschall-Reinigungsgerät. https://www.elma-ultrasonic.com/fileadmin/downloads/Produktprofile/Produktprofile_DE/Ultraschallgeraete/Elmasonic_S/PP_Elmasonic_S30H_DE.pdf. Accessed 14 Sep 2020

77 Schmalenberg M, Sallamon F, Haas C et al (2020) Temperature-controlled minichannel flow-cell for non-invasive particle measurements in solid-liquid flow. In: Proceedings of the ASME 18th International Conference on Nanochannels, Microchannels, and Minichannels 2020. American Society of Mechanical Engineers Digital Collection; The American Society of Mechanical. https://doi.org/10.1115/ICNMM2020-1062

78 Borchert C, Sundmacher K (2011) Crystal aggregation in a flow tube: image-based observation. Chem Eng Technol 34:545–556. https://doi.org/10.1002/ceat.201000465

79 Huo Y, Liu T, Liu H et al (2016) In-situ crystal morphology identification using imaging analysis with application to the L-glutamic acid crystallization. Chem Eng Sci 148:126–139. https://doi.org/10.1016/j.ces.2016.03.039

80 Kumar V, Mridha M, Gupta AK et al (2007) Coiled flow inverter as a heat exchanger. Chem Eng Sci 62:2386–2396. https://doi.org/10.1016/j.ces.2007.01.032

81 (2013) VDI-Wärmeatlas. Springer Berlin Heidelberg, Berlin

82 Emig G, Klemm E (2017) Chemische Reaktionstechnik. Springer Berlin Heidelberg, Berlin

83 Gelhausen MG, Kurt SK, Kockmann N (2014) Mixing and heat transfer in helical capillary flow reactors with alternating bends. In: ASME 2014 12th International Conference on Nanochannels, Microchannels, and Minichannels collocated with the ASME 2014 4th Joint US-European Fluids Engineering Division Summer Meeting. ASME

84 Wohlgemuth K, Schembecker G (2013) Modeling induced nucleation processes during batch cooling crystallization: A sequential parameter determination procedure. Comput Chem Eng 52:216–229. https://doi.org/10.1016/j.compchemeng.2012.12.001

85 Lorimer JP, Mason TJ, Fiddy K (1991) Enhancement of chemical reactivity by power ultrasound: an alternative interpretation of the

hot spot. Ultrasonics 29:338–343. https://doi.org/10.1016/0041-624X(91)90032-4
86 Valitov G, Jamshidi R, Rossi D et al (2020) Effect of acoustic streaming on continuous flow sonocrystallization in millifluidic channels. Chem Eng J 379:122221. https://doi.org/10.1016/j.cej.2019.122221
87 Durga KKH, Selvarajan P, Shanthi D (2012) Nucleation kinetics, XRD and SHG studies of L-Alanine single crystals grown at different supersaturation levels. Int J Curr Res Rev 2012:68–77
88 Hofmann G (ed) (2004) Kristallisation in der industriellen Praxis. Wiley-VCH, Weinheim
89 Furuta M, Mukai K, Cork D et al (2016) Continuous crystallization using a sonicated tubular system for controlling particle size in an API manufacturing process. Chem Eng Process Process Intensif 102:210–218. https://doi.org/10.1016/j.cep.2016.02.002
90 Eder RJP, Radl S, Schmitt E et al (2010) Continuously seeded, continuously operated tubular crystallizer for the production of active pharmaceutical ingredients. Cryst Growth Des 10:2247–2257. https://doi.org/10.1021/cg9015788
91 Eder RJP, Schmitt EK, Grill J et al (2011) Seed loading effects on the mean crystal size of acetylsalicylic acid in a continuous-flow crystallization device. Cryst Res Technol 46:227–237. https://doi.org/10.1002/crat.201000634
92 Wiedmeyer V, Anker F, Bartsch C et al (2017) Continuous crystallization in a helically coiled flow tube: analysis of flow field, residence time behavior, and crystal growth. Ind Eng Chem Res 56:3699–3712. https://doi.org/10.1021/acs.iecr.6b04279
93 Wiedmeyer V, Voigt A, Sundmacher K (2017) Crystal population growth in a continuous helically coiled flow tube crystallizer. Chem Eng Technol 40:1584–1590. https://doi.org/10.1002/ceat.201600530

Mira Schmalenberg studied Chemical Engineering at TU DortmundUniversity. In November 2017, she completed her master thesis on the design ofa modular continuous-flow tubular cooling crystallizer for process developmentand small-scale production at the Laboratory of Equipment Design. In February2018, she started as a research assistant in the ENPRO2.0-TeiA("Trennverfahren mit effizienten und intelligenten Apparaten'') project at theLaboratory of Equipment Design. Her focus is theinvestigation of small scale continuous cooling crystallizers.

Lena K. Weick studied Chemical Engineering at TU DortmundUniversity since 2013. She graduated with the master thesis "Investigation ofdifferent operating modes of a coiled tube cooling crystallizer" at theLaboratory of Equipment Design in 2020.

Norbert Kockmann studiedmechanical engineering at the Technical University of Munich and completed hisDr.-Ing. in process engineering at the University in Bremen. After 5 years in chemicalindustry as project manager he joined Freiburg University, IMTEK in 2001 asgroup leader for micro process engineering. In 2007, Dr. Kockmann joined LonzaLtd., Visp, Switzerland, as senior scientist responsible for continuous flowprocesses and microreactor technology. In April 2011, Norbert Kockmann wasappointed as full professor for equipment design at TU Dortmund University,Germany. His research interests are on small-scale device for continuouschemical processes, modular design, and process intensification. His workincludes fundamental investigations of small-scale multiphase flow, modellingand simulation accompanied by modern sensing technology and machine-learningmethods.